

# Tri-band Aperture-shared Antenna Array Using Scalable FSS-based Electromagnetic Transparent Structure

Yongzheng Li, *Student Member, IEEE*, Wanchen Yang, *Senior Member, IEEE*, Quan Xue, *Fellow, IEEE* and Wenquan Che, *Fellow, IEEE*

**Abstract**—A novel dual-band electromagnetic transparent structure (DBTS) is firstly proposed and used to realize a tri-band aperture-shared antenna array. The DBTS achieves two tunable electromagnetic transparent frequency bands by periodically loading capacitive patches and meander lines to an inductive strip. Meanwhile, the DBTS features flexible frequency band scalability by loading additional serial  $L$ - $C$  tanks. In tri-band aperture-shared arrays, the low-band (LB) dipole induces a deterioration in the radiation pattern of the middle-band (MB) and high-band (HB) antennas as a consequence of the shielding effects. To address this issue, the DBTS is utilized to construct the LB dipole, with its electromagnetic transparent bands allocated at MB and HB simultaneously. Consequently, a tri-band aperture-shared array is realized by combining the LB dipole with a dual-band subarray that operates at MB and HB within a shared aperture. The proposed array realizes an aperture-shared operation within the frequency ranges covering 0.65-0.88GHz (LB), 1.92-2.18GHz (MB) and 3.3-3.8GHz (HB). The LB dipole induces minimal shielding to the MB and HB antennas, resulting in their restored radiation performance with broadside gain deviation of less than 0.6dB.

**Index Terms**—Aperture-shared antenna array, base-station antenna, electromagnetic transparent structure, radiation pattern distortion.

## I. INTRODUCTION

Multi-band aperture-shared antenna arrays are a promising solution for 2G-5G communication standards compatibility, reducing costs and saving space in the next-generation communication system. However, these arrays suffer from strong interference across different frequency bands, resulting in radiation performance deterioration.

This work was supported in part by the National Natural Science Foundation of China under Grant 62321002. (*Corresponding author: Wenquan Che*)

Y. Li, Q. Xue and W. Che are with the Guang g Provincial Key Laboratory of Millimeter-Wave and Terahertz, Guangdong-Hong Kong-Macao Joint Laboratory for Millimeter-Wave and Terahertz, School of Electronic and Information Engineering, South China University of Technology, Guangzhou 510641, China. (e-mail: [eclyz@ieee.org](mailto:eclyz@ieee.org), [eeqxue@scut.edu.cn](mailto:eeqxue@scut.edu.cn), [eeqwche@scut.edu.cn](mailto:eeqwche@scut.edu.cn)).

W. Yang is with the College of Electronic and Information Engineering, Nanjing University of Aeronautics and Astronautics, Nanjing 211106, China, and also with the Guangdong Key Laboratory of Millimeter-Waves and Terahertz, the School of Electronic and Information Engineering, South China University of Technology, Guangzhou 510641, China. (e-mail: [yangwanchen@126.com](mailto:yangwanchen@126.com)).

To alleviate this problem, many effective multi-band aperture-shared approaches have been proposed [1]–[19]. In the top-bottom scheme used in [1–4], the HB antenna is placed above the LB antenna, with a low-pass surface inserted between them. This surface performs as a reflector for the HB antenna and as a capacitive parasitic structure for the LB antenna. This scheme can achieve wide bandwidth but the feeding line of the HB antenna affects the performance of the LB antenna. Loading chocks [6]–[9], [15]–[17] can effectively suppress induced currents on LB radiators. However, these chocks degrade the impedance matching of the LB antenna. Loading slots [10] to make the scattering of LB radiator self-cancelled can also greatly mitigate the blockage effect. This method has the potential for integrating more frequency bands, but the shape and position of the slots must be carefully optimized. Besides, Slot-ring FSS was constructed on the arm of the LB dipole in [4], [11]–[13], [18], [19], but the size of LB radiator needs to be compromised with the dimension of the FSS. Therefore, further research is needed to develop a multi-band aperture-shared method that can integrate more frequency bands without degrading the performance of the LB antenna.

In this work, a dual-band electromagnetic transparent structure (DBTS) is proposed, capable of producing two tunable electromagnetic transparent bands. The proposed DBTS features flexible frequency band scalability by adding  $L$ - $C$  tanks to its equivalent circuit. To minimize the shielding effect caused by the LB dipole on the MB and HB antennas in the tri-band aperture-shared array, the proposed DBTS is utilized to construct the LB dipole. Consequently, a tri-band aperture-shared antenna array is realized by combining the LB dipole with a dual-band sub-array that operates in MB and HB. The tri-band array features minimal shielding effects, a simple structure, and flexible frequency band scalability.

## II. ELECTROMAGNETIC TRANSPARENT STRUCTURE BASED ON FSS

As illustrated in Fig. 1, the proposed DBTS is originated from one thin strip, which is equivalent to a shunt inductor  $L_p$ , and termed with *Case-A*. Then *Case-B* is obtained from *Case-A* by loading the periodical meander line on the opposite side of the laminate, and this introduces a serial  $L_s$ - $C_s$  tank in parallel with the  $L_p$ . *Case-C* represents the proposed DBTS, which incorporates capacitive patches on the basis of *Case-B*,

> REPLACE THIS LINE WITH YOUR MANUSCRIPT ID NUMBER (DOUBLE-CLICK HERE TO EDIT) <

these capacitive patches induce the serial tank  $L_{s1}$ - $C_{s1}$ . Note that the capacitive patches are etched on both side of two additional laminates, the air spacing between the laminates is modeled with transmission lines. The value of  $L_p$  and  $C_{s1}$  are calculated from the dimensions of structure using the equations in [20], while the  $L_{s1}$ ,  $L_s$  and  $C_s$  are extracted using the method in [21]. Furthermore, slight parameter tuning is performed to improve accuracy.

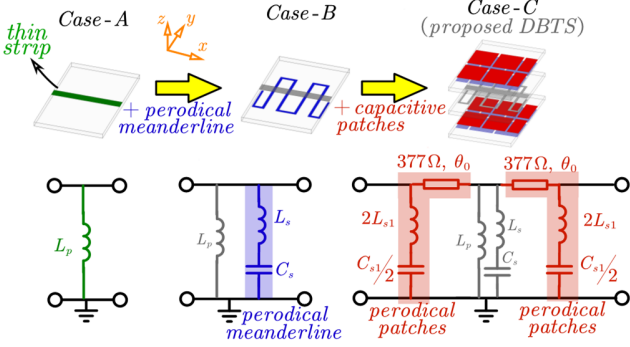


**Fig. 1.** Configuration and equivalent circuit for *Case-A* to *Case-C*. The circuit parameters:  $L_{s1}=0.1\text{nH}$ ,  $C_{s1}=0.28\text{pF}$ ,  $L_p=8.2\text{nH}$ ,  $L_s=45.7\text{nH}$ ,  $C_s=0.0915\text{pF}$ ,  $\theta_0=10.56^\circ$  @  $3.55\text{GHz}$ .

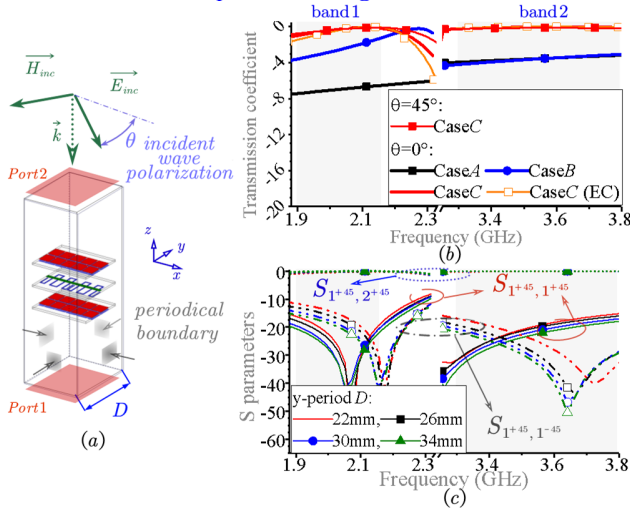


**Fig. 2.** (a) Configuration of the simulation model, (b) Transmission coefficient for *Case-A* to *Case-C*, (c) S parameters for *Case-C* with varies y-period  $D$ .

To validate the equivalent circuit and further reveal the operating mechanism, the transmission coefficients are compared among *Case-A* to *Case-C*. The simulation model, as shown in Fig. 2(a), uses a periodic boundary surrounding the structures. The angle between the polarization direction of the incident field and the  $x$ -axis is  $\theta$ . Fig. 2(b) shows that when  $\theta=0^\circ$ , *Case-A* exhibits poor performance with a transmission loss exceeding 3dB, while *Case-B* has a single passband near 2.3 GHz; *Case-C* has two distinct passbands denoted as *band 1* and *band 2*, spanning 1.92-2.18 GHz and 3.3-3.8 GHz, respectively, with a transmission coefficient over -0.92dB. Meanwhile, the full-wave and equivalent circuit simulation results for *Case-C* are consistent, confirming the high accuracy of the circuit model. Therefore, the *band 1* is created

by the interaction between the thin strip and the periodic meander line, while *band 2* is generated by the capacitive patch. Therefore, the number of passbands can be increased by adding serial  $L$ - $C$  tanks.

Notably, although the proposed DBTS resonates only along the  $x$ -axis, it also exhibits a high transmission coefficient for an incident wave polarized in  $\theta=45^\circ$ , as shown in Fig. 2(b). This is attributed to the small electromagnetic size along the non-resonant  $y$ -axis. Meanwhile, Fig. 2(c) compares the S parameters of the DBTS for different periodical boundary widths  $D$  in the  $y$  direction. The resonance frequencies remain nearly unchanged with varying  $y$ -periods, indicating that increasing the  $y$ -period has minimal impact on the performance of the DBTS.

### III. TRI-BAND APERTURE-SHARED ANTENNA ARRAY

In the tri-band aperture-shared antenna arrays, the shielding effect caused by LB antenna at MB and HB presents a significant challenge. To resolve this issue, the proposed DBTS is used to construct an LB dipole antenna, which is then combined with a dual-band sub-array operating at MB and HB to create a tri-band aperture-shared antenna array.

#### A. Configuration of the Tri-band Aperture-shared Antenna Array

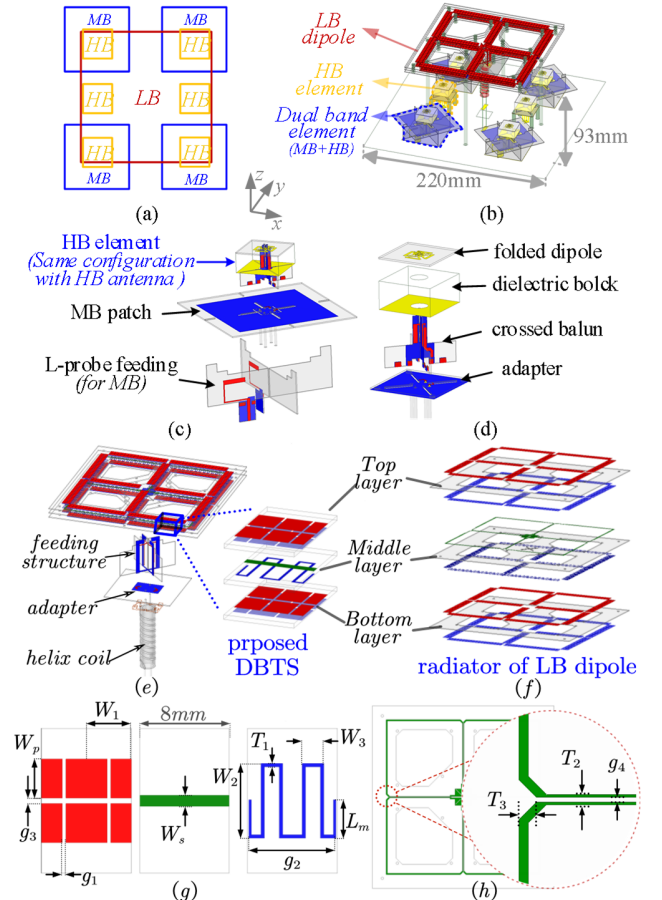


**Fig. 3.** Configuration of the triband aperture-shared array: (a) Topology sketch, (b) 3D view. Configurations for: (c) The dual-band antenna, (d) The high-band antenna. (e) The LB antenna (f) LB

> REPLACE THIS LINE WITH YOUR MANUSCRIPT ID NUMBER (DOUBLE-CLICK HERE TO EDIT) <

radiator. The dimensions of: (g) The DBTS and (h) Top layer of the LB radiator. The key parameters:  $W_1=2.95\text{mm}$ ,  $W_2=6.7\text{mm}$ ,  $W_3=1.93\text{mm}$ ,  $W_5=20\text{mm}$ ,  $W_p=3.5\text{mm}$ ,  $W_s=1\text{mm}$ ,  $L_m=3.45\text{mm}$ ,  $r_1=5\text{mm}$ ,  $r_2=3\text{mm}$ ,  $g_1=0.25\text{mm}$ ,  $g_2=7.75\text{mm}$ ,  $g_3=g_4=0.5\text{mm}$ ,  $T_1=0.3\text{mm}$ ,  $T_2=1.1\text{mm}$ ,  $T_3=2\text{mm}$ .

As shown in Fig. 3(a-b), the tri-band antenna array consists of an LB dipole and a dual-band sub-array operating in the MB and HB. The dual-band sub-array is arranged with four dual-band antennas interleaved with two HB antennas. The array spacing is 100 mm in the x-direction. In the y-direction, the spacing is 60 mm for the HB while 120 mm for the MB, respectively. The configurations of the dual-band and the HB antenna are shown in Fig. 3(c-d). The dual-band antenna consists of one HB element stacked upon one MB patch antenna, while the HB element shares the same configuration with the HB antenna shown in Fig. 3(d). The radiator of LB dipole is illustrated in Fig. 3(e-h), which is constructed by the proposed DBTS to mitigate the shielding effect. Noting that the DBTS with coupled line is employed in the middle part of the dipole, the coupled-line width is appropriately designed so that the coupled-line DBTS operates within the same passbands as the single-line one. All the substrates used in the antenna array design are Rogers Kappa438 laminates with thickness of 0.508mm and permittivity of 4.38.

#### B. Scattering Suppression Effect of the Proposed LB Dipole

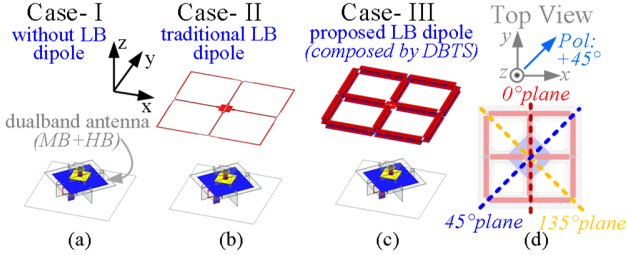


**Fig. 4.** Configurations of the three cases: (a) *Case-I*: without LB dipole, (b) *Case-II*: traditional LB dipole, (c) *Case-III*: LB dipole composed by the DBTS; (d) Schematic on observation plane cuts in top view.

To demonstrate the scattering suppression effect of the proposed LB antenna at MB and HB, three cases are considered, as illustrated in Fig. 4. In *Case-I*, only the dual-band antenna operating at MB and HB is considered. In *Case-II*, a traditional LB dipole is set above the dual-band antenna coaxially. The *Case-III* is like *Case-II*, but using the LB dipole composed of the DBTS instead. The 3D radiation patterns for the three cases are compared in Fig. 5. Compared to *Case-I*, radiation pattern deterioration is observed in *Case-II*, indicating a significant shielding effect caused by the traditional LB dipole. In contrast, the 3D radiation patterns in *Case-I* and *Case-III* are highly similar for both MB and HB. This similarity demonstrates that the proposed LB dipole effectively suppresses the shielding effect, preserving the radiation pattern as if no LB dipole were present.

To quantitatively evaluate the reduction in shielding effect, Fig. 6 compares the radiation patterns for these three cases. Considering the feature of symmetry, only three plane cuts (azimuth angle =  $0^\circ$ ,  $45^\circ$ , and  $135^\circ$ ) of the patterns are

illustrated. In *Case-II*, the broadside gain is about 2 dB lower than in *Case-I* for MB, and approximately 1 dB lower than in *Case-I* for HB. In contrast, the radiation patterns of *Case-III* are very similar to those of *Case-I*, with a broadside gain difference of less than 0.5 dB for both MB and HB. Therefore, incorporating the DBTS with the dipole effectively restores the radiating performance.

Noting that although the DBTS is designed under periodic boundary conditions, and the DBTS in the LB dipole operates with an open boundary in the non-resonant direction, the passband characteristics remain nearly unchanged in both cases. This is because the DBTS performance is not sensitive to the non-resonant direction period, while the open boundary represents the limiting case of an infinitely large period. Consequently, the DBTS designed under periodic boundaries remains suitable for integration into the LB dipole [14].

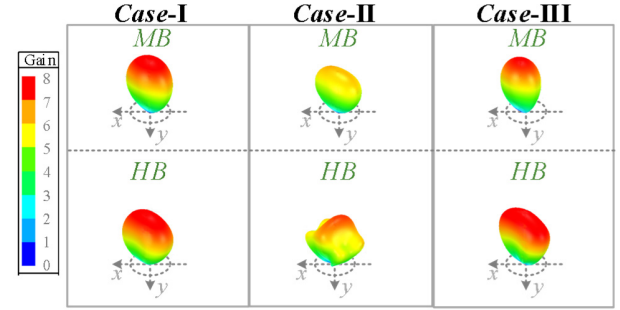


**Fig. 5.** 3D radiation patterns at HB (3.55GHz) and MB (2.05GHz) for *Case-I* to *Case-III*.

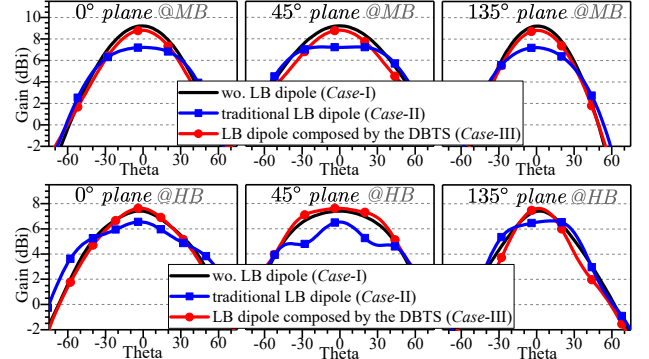


**Fig. 6.** Radiation patterns for *Case-I*, II, III when the azimuth angle is respectively equal to  $0^\circ$ ,  $45^\circ$  and  $135^\circ$  at HB and MB.

## IV. RESULTS AND DISCUSSION

For verification of the design, the proposed tri-band aperture-shared antenna array is fabricated and measured. The prototype and ports distribution are illustrated in Fig. 7(a)

#### A. S Parameters

The S Parameters of the proposed antenna array is measured with R&S-ZVA40 vector network analyzer. Only the performance of ports  $H_1^+$ ,  $H_2^+$ ,  $M_1^+$ ,  $L^+$  are shown due to array symmetry. As shown in Fig. 7(b), the measured reflection coefficients of ports  $L^+$ ,  $M_1^+$ ,  $H_1^+$  and  $H_2^+$  are lower than -10dB. Some difference exists between the simulated and measured reflection coefficient of  $H_1^+$ , which is probably due to the errors induced in soldering the SMA

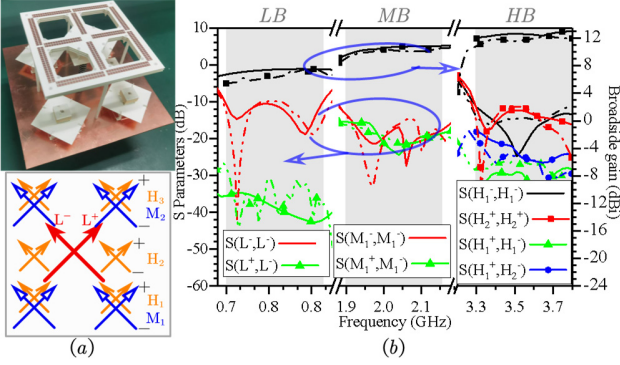
> REPLACE THIS LINE WITH YOUR MANUSCRIPT ID NUMBER (DOUBLE-CLICK HERE TO EDIT) <

TABLE I  
COMPARISON BETWEEN CURRENTLY MULTIBAND APERTURE SHARED ANTENNA ARRAYS

works	Operating bands (GHz)	LB radiator shielding effect reduction Method	Capability of integrating more bands in same aperture	Max. broadside gain deviation of elements in array* (dB)	Complexity
[4]	0.69–0.96 (32.7%) 1.8–2.7 (40%) 3.3–3.8 (14%)	high-stop surface + top-bottom scheme	low	Not available	high (structural)
[9]	0.79–0.96 (19.4%) 1.71–2.17 (23.7%) 3.4–3.6 (5.7%)	SSR + chock	medium	~0.55 (MB) ~1.23(HB)	medium
[10]	0.69–0.96 (32.7%) 1.7–2.4 (34.1%)	slot loading	medium	~0.83	high (design procedure)
<b>This work</b>	<b>0.65–0.88 (30%)</b> <b>1.92–2.18 (12.7%)</b> <b>3.3–3.8 (14%)</b>	<b>FSS-based DBTS</b>	<b>high</b>	<b>0.57(MB)</b> <b>0.5(HB)</b>	<b>low</b>

\*The broadside gain deviation of the other works is evaluated from the figure in their articles.

connector to the coaxial cable. Nevertheless, good agreement is observed between the simulated and measured results of the other ports.



**Fig. 7.** (a) Prototype and port distribution of the proposed array; (b) Reflection coefficient and isolation within same element for ports  $L^+$ ,  $M_1^+$ ,  $H_1^+$  and  $H_2^+$  (left side), along with broadside gains (right side) of the array for each band. (Note that simulated results are presented with solid lines while measured results are in dashed-dot lines)

### B. Radiation Patterns

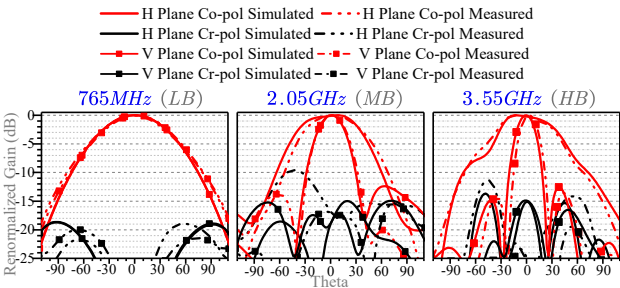


**Fig. 8.** Simulated and measured renormalized radiation pattern in horizontal and vertical plane at LB, MB and HB, respectively.

The radiation pattern of the proposed tri-band aperture-shared antenna array is measured with the MVG near-field chamber. Note that the antenna array is proposed for MIMO applications, and is fed in columns during the measurement. The measured broadside gains for each operating band are shown in the right side of Fig. 7(b). As we see, some difference within 0.5 to 1dB exists between simulation and measurement, probably caused by loss of the RG047 cables and SMA adaptors. Measured and simulated renormalized

radiation patterns at the center frequencies in the three bands are shown in Fig. 8, good agreement is observed.

For further demonstration, a comparison with other reported multiband aperture shared antenna arrays is shown in Table. I. The antenna array proposed in [4] has wider bandwidth within the three frequency bands. However, the top-bottom configuration is difficult to scale for additional frequency bands integration due to the complexity and scattering caused by the HB feeding structures. The tri-band array proposed in [9] has a wider bandwidth in MB but narrower in HB and LB, the combination of SSRs and chocks loading for LB radiator scattering suppression limits the bandwidth of LB dipole. In addition, when more frequency bands are required to be integrated, the chocks and SSRs for lower bands can also cause scattering in the higher bands, making it difficult to integrate additional frequency bands using this method. Slot loading method used in [10] allows for the integration of more frequency bands by adding different types of slots onto the radiator. However, the shape and position of each slot must be carefully designed, leading to a more complex design process for the LB dipole. The FSS-based DBTS proposed in this work features low broadside gain deviation and high capability of frequency bands extension with a simple structure, indicating one favorable solution in multiband-aperture shared antenna array design.

### V. CONCLUSION

One novel DBTS is proposed and realized in this work, which features flexible frequency bands scalability. To reduce the radiation pattern distortion of the MB and HB antennas caused by the shielding effect of the LB dipole in a tri-band aperture-shared array, the proposed DBTS is employed to construct the LB dipole. A tri-band aperture-shared antenna array is then achieved by integrating the proposed LB dipole with a dual-band sub-array operating at MB and HB. As a result, the radiation performance of the MB and HB antennas is effectively restored, with the broadside gain deviation caused by the shielding effect below 0.6dB.

> REPLACE THIS LINE WITH YOUR MANUSCRIPT ID NUMBER (DOUBLE-CLICK HERE TO EDIT) <

#### REFERENCES

- [1] Y. Zhu, Y. Chen, and S. Yang, "Helical Torsion Coaxial Cable for Dual-Band Shared-Aperture Antenna Array Decoupling," *IEEE Trans. Antennas Propag.*, vol. 68, no. 8, pp. 6128–6135, Aug. 2020, doi: 10.1109/TAP.2020.2986725.
- [2] Y. Chen, J. Zhao, and S. Yang, "A Novel Stacked Antenna Configuration and its Applications in Dual-Band Shared-Aperture Base Station Antenna Array Designs," *IEEE Trans. Antennas Propag.*, vol. 67, no. 12, pp. 7234–7241, Dec. 2019, doi: 10.1109/TAP.2019.2930136.
- [3] Y. Zhu, Y. Chen, and S. Yang, "Decoupling and Low-Profile Design of Dual-Band Dual-Polarized Base Station Antennas Using Frequency-Selective Surface," *IEEE Trans. Antennas Propag.*, vol. 67, no. 8, pp. 5272–5281, Aug. 2019, doi: 10.1109/TAP.2019.2916730.
- [4] D. He, Y. Chen, and S. Yang, "A Low-Profile Triple-Band Shared-Aperture Antenna Array for 5G Base Station Applications," *IEEE Trans. Antennas Propag.*, vol. 70, no. 4, pp. 2732–2739, Apr. 2022, doi: 10.1109/TAP.2021.3137486.
- [5] Y. Qin, R. Li, Q. Xue, X. Zhang, and Y. Cui, "Aperture-Shared Dual-Band Antennas With Partially Reflecting Surfaces for Base-Station Applications," *IEEE Trans. Antennas Propag.*, vol. 70, no. 5, pp. 3195–3207, May 2022, doi: 10.1109/TAP.2021.3137448.
- [6] X. W. Dai, C. Ding, F. Zhu, L. Liu, and G. Q. Luo, "Broadband Dual-Polarized Element With Rotated Sleeve Arms for Compact Dual-Band Antenna," *IEEE Antennas Wirel. Propag. Lett.*, vol. 20, no. 12, pp. 2519–2523, Dec. 2021, doi: 10.1109/LAWP.2021.3117037.
- [7] H.-H. Sun, H. Zhu, C. Ding, B. Jones, and Y. J. Guo, "Scattering Suppression in a 4G and 5G Base Station Antenna Array Using Spiral Chokes," *IEEE Antennas Wirel. Propag. Lett.*, vol. 19, no. 10, pp. 1818–1822, Oct. 2020, doi: 10.1109/LAWP.2020.3019930.
- [8] H.-H. Sun, C. Ding, H. Zhu, B. Jones, and Y. J. Guo, "Suppression of Cross-Band Scattering in Multiband Antenna Arrays," *IEEE Trans. Antennas Propag.*, vol. 67, no. 4, pp. 2379–2389, Apr. 2019, doi: 10.1109/TAP.2019.2891707.
- [9] Y.-L. Chang and Q.-X. Chu, "Suppression of Cross-Band Coupling Interference in Tri-Band Shared-Aperture Base Station Antenna," *IEEE Trans. Antennas Propag.*, vol. 70, no. 6, pp. 4200–4214, Jun. 2022, doi: 10.1109/TAP.2021.3138531.
- [10] Y.-S. Wu, Q.-X. Chu, and H.-Y. Huang, "Electromagnetic Transparent Antenna With Slot-Loaded Patch Dipoles in Dual-Band Array," *IEEE Trans. Antennas Propag.*, vol. 70, no. 9, pp. 7989–7998, Sep. 2022, doi: 10.1109/TAP.2022.3164194.
- [11] D. He, Q. Yu, Y. Chen, and S. Yang, "Dual-Band Shared-Aperture Base Station Antenna Array With Electromagnetic Transparent Antenna Elements," *IEEE Trans. Antennas Propag.*, vol. 69, no. 9, pp. 5596–5606, Sep. 2021, doi: 10.1109/TAP.2021.3061151.
- [12] Y. Zhu, Y. Chen, and S. Yang, "Cross-Band Mutual Coupling Reduction in Dual-Band Base-Station Antennas With a Novel Grid Frequency Selective Surface," *IEEE Trans. Antennas Propag.*, vol. 69, no. 12, pp. 8991–8996, Dec. 2021, doi: 10.1109/TAP.2021.3098514.
- [13] G.-N. Zhou, B.-H. Sun, Q.-Y. Liang, S.-T. Wu, Y.-H. Yang, and Y.-M. Cai, "Triband Dual-Polarized Shared-Aperture Antenna for 2G/3G/4G/5G Base Station Applications," *IEEE Trans. Antennas Propag.*, vol. 69, no. 1, pp. 97–108, Jan. 2021, doi: 10.1109/TAP.2020.3016406.
- [14] S. J. Yang, Y. Yang, and X. Y. Zhang, "Low Scattering Element-Based Aperture-Shared Array for Multiband Base Stations," *IEEE Trans. Antennas Propag.*, vol. 69, no. 12, pp. 8315–8324, Dec. 2021, doi: 10.1109/TAP.2021.3083760.
- [15] W. Niu, B. Sun, G. Zhou, and Z. Lan, "Dual-Band Aperture Shared Antenna Array With Decreased Radiation Pattern Distortion," *IEEE Trans. Antennas Propag.*, vol. 70, no. 7, pp. 6048–6053, Jul. 2022, doi: 10.1109/TAP.2022.3161267.
- [16] H.-H. Sun, B. Jones, Y. J. Guo, and Y. H. Lee, "Suppression of Cross-Band Scattering in Interleaved Dual-Band Cellular Base-Station Antenna Arrays," *IEEE Access*, vol. 8, pp. 222486–222495, 2020, doi: 10.1109/ACCESS.2020.3043578.
- [17] S. J. Yang, R. Ma, and X. Y. Zhang, "Self-Decoupled Dual-Band Dual-Polarized Aperture-Shared Antenna Array," *IEEE Trans. Antennas Propag.*, vol. 70, no. 6, pp. 4890–4895, Jun. 2022, doi: 10.1109/TAP.2021.3137531.
- [18] X. Liu *et al.*, "A Mutual-Coupling-Suppressed Dual-Band Dual-Polarized Base Station Antenna Using Multiple Folded-Dipole Antenna," *IEEE Trans. Antennas Propag.*, vol. 70, no. 12, pp. 11582–11594, Dec. 2022, doi: 10.1109/TAP.2022.3209177.
- [19] Y. Jia, H. Zhai, J. Yin, Y. Wang, and Y. Liu, "A Quadruple-Band Shared-Aperture Antenna Array With Multiband Radiation Pattern Restorations," *IEEE Trans. Antennas Propag.*, vol. 72, no. 10, pp. 7722–7735, Oct. 2024, doi: 10.1109/TAP.2024.3439874.
- [20] S. M. A. Momeni Hasan Abadi, M. Li, and N. Behdad, "Harmonic-Suppressed Miniaturized-Element Frequency Selective Surfaces With Higher Order Bandpass Responses," *IEEE Trans. Antennas Propag.*, vol. 62, no. 5, pp. 2562–2571, May 2014, doi: 10.1109/TAP.2014.2303822.
- [21] F. Costa, A. Monorchio, and G. Manara, "An Overview of Equivalent Circuit Modeling Techniques of Frequency Selective Surfaces and Metasurfaces," vol. 29, no. 12, 2014.